

03,09,12

# Multi-zone resonance spectrometry of inelastic electron scattering of light and the manifestation of strong spin-orbit interaction in nanostructures with quantum dots

© V.V. Toporov, B.H. Bairamov<sup>¶</sup>

Ioffe Institute,  
St. Petersburg, Russia

<sup>¶</sup>E-mail: bairamov@mail.ioffe.ru

Received March 23, 2023

Revised April 4, 2023

Accepted April 4, 2023

Highly sensitive methods of inelastic light scattering spectrometry have been developed to detect individual photons in the visible and near-infrared spectral ranges (0.4–1.35)  $\mu\text{m}$ . Precision optical measurements of vibrational and electronic states of nanostructures with quantum objects are performed, using the example of quantum-dimensional nanoheterostructures (311) In *si*-GaAs/InAs with InAs quantum dots. A distinctive attractive feature of such structures with a degenerate valence band of symmetry  $\Gamma_8$  is the presence of a strong spin-orbit interaction. In this case, the intrinsic moment of the holes can effectively interact with the electric field of the incident light wave. It was found that such interaction causes intense luminescence and inelastic scattering of the light wave in the IR region of the 0.9–1.35  $\mu\text{m}$  spectrum. Effective generation of nonequilibrium electron-hole ( $e-h$ ) plasma with concentrations  $n = p = 1.0 \cdot 10^{17} \text{ cm}^{-3}$  and  $T_e = T_h = 25 \text{ K}$ , was revealed under resonant excitation conditions, while the lattice temperature  $T_L = 5.1 \text{ K}$ . New mechanisms have been discovered for the formation of an abnormally intense integration spectrum of multiplex inelastic light scattering of a rather complex shape formed by various separable resonant contributions of the processes of quasi-elastic scattering by charge carriers, light scattering by acoustic plasmons of electron-hole plasma, as well as inelastic intra- and inter-band light scattering by heavy holes. It has been established that the anomalous intensity gain of such multi-zone selective resonant light scattering is more than  $10^5$  times higher than the intensity of Thomson light scattering on individual charge carriers. There is agreement between the estimated calculated and experimental spectra, and for the most part for the difficult-to-interpret significant width of the observed light scattering line. It is shown that new mechanisms of various contributions to the formation of scattered photon radiation are important diagnostic elements that are clearly manifested in the spectra of the resulting enhanced inelastic light scattering.

**Keywords:** nanostructures, quantum objects, resonant scattering of light by charge carriers, exchange interaction, plasma diagnostics.

DOI: 10.21883/PSS.2023.05.56041.41

## 1. Introduction

In terms of quantum-mechanical positions, the inelastic light scattering process is caused by transition of lattice atom electrons from their ground state into excited state that occurs through intermediate electronic states of electron-hole pairs induced by incident exciting radiation photons on the sample. Therefore, the intermediate electronic states play the main role by forming quantum paths that determine the nature of important nonresonance and resonance behavior mechanisms of light scattering processes, and of interference in the exciting and scattered paths. In early 1980s, Ioffe Institute started the research of a new type of inelastic resonant light scattering. Alternatively to the traditionally studied and usually interpreted two-band resonance enhancement of inelastic light scattering intensity (see, for example, [1–5]), a multiband resonance enhancement of inelastic light scattering intensity was predicted and discovered [6,7]. Initially, the multiband nature of the enhancement was justified and experimentally proved

for Mandelstam–Brillouin inelastic resonant light scattering by acoustic phonons with wave vectors corresponding to point  $\Gamma$  of the Brillouin zone using ZnSe crystals having a zinc blende-type structure [6,7]. In addition, all exciton correlations both for interband and band-to-band transitions between conduction band  $\Gamma_6$ , fourfold degenerate valence band  $\Gamma_8$  and doubly degenerate zone  $\Gamma_7$  split off by spin-orbital interaction were considered for the first time. Moreover, real Wannier–Mott exciton states belonging both to discrete hydrogen-like exciton bands and continuous spectrum were also addressed for the first time as intermediate virtual electronic states involved in the scattering processes. The obtained reliable and high-accuracy experimental dependences of resonant light scattering intensity by such acoustic lattice vibrations vs. exciting radiation quantum energy measured with high spectral resolution using scanned multi-pass Fabry–Perot interferometer were found to be insufficiently well described on the basis of widely used two-band light scattering model which was addressed theoretically by Loudon [1]. Then,

the same approach and conclusions made on the basis of [6,7] were expanded and proved by detailed study of inelastic resonant light scattering by optical phonons using AgJ crystals [8]. And in this case, it was also clearly found [8] that the obtained experimental dependences of inelastic resonant light scattering intensity by optical lattice vibrations vs. exciting radiation quantum energy were still insufficiently well described by Loudon's two-band model [1]. In addition, Loudon's theoretical model does not include Coulomb interaction by intermediate electronic states. Later, they were included by Ganguly and Birman [2] and Martin [3]. They considered weak exciton-photon interaction and derived an expression for inelastic (Raman) resonant light scattering tensor for deformation potential and Frelich electron-phonon interaction. Similar calculations were also made in [4] using Green's functions. And all these studies [1–5] addressed the inelastic resonant light scattering mechanism with fundamental transition only via one valence band and one conduction band. Such resonant scattering model does not take in account the Coulomb intermediate electronic state interaction and address these electronic states as free electron-hole pair states. The theory multiband inelastic resonant light scattering by lattice vibrations introduced by us [6–8] described in detail hydrogen-like exciton states not addressed before as intermediate electronic states. These states belong to discrete exciton bands and continuous spectrum as well as to high-level valence bands [6–8].

In the following years, the multiband inelastic resonant light scattering theory and approaches addressed in [6–8] were used and supported in [9,10]. These studies, including the approaches developed in [6–8], recalculated the results of the previous studies of resonant light scattering for some most important semiconductors from  $A^3B^5$  group [9,10]. Afterwards, extensive expansion of the multiband resonant light scattering theory applications also proved its consistency and suitability for many main groups of semiconductor materials — from bulk (for example [9,10]) to low-dimensional nanostructures (for example, [11]). The multiband resonant light scattering by localized optical phonons has been recently found in the isolated nanocrystalline quantum dots  $nc\text{-Si/SiO}_2$  [12]. We have also shown recently that in nitrogen-doped diamond crystals, formation of many electronic levels may cause vivid manifestation of the multiband resonant light scattering mechanism [13–15]. Results of the resonant light scattering studies on optical phonons for the assembly of optically active NV centers in diamond crystals were presented. Diamond crystals with such centers are of high interest due to their potential use in quantum technology. The data obtained in [13–15] show that strong enhancement of the inelastic resonant light scattering intensity by optical phonons was detected. Using a diamond single-crystal oriented along (100) axis and containing  $[N_s]^0 < 1$  ppm of nitrogen impurities as an example, it was found that the resonance processes with two electronic transitions play the leading role for optically active nitrogen impurity centers: (1) with zero-

phonon lines for neutral  $NV_0$ -center at 575.468 nm in the input scattering channel with laser emission excitation  $\lambda_i = 532.070$  nm and (2) for negatively charged  $NV^-$ -center at 637.874 nm in the output scattering channel with laser emission excitation  $\lambda_i = 632.817$  nm. According to the measurements of optical-phonon light scattering intensities taking into account the instrument corrections for energy dependence of the spectrometer sensitivity, spectral slit widths, optical absorption and  $(1/\lambda_i)^4$ -dependence of scattered light intensity, unusual enhancement of the optical-phonon resonant light scattering line intensity by more than 2.5 times was detected when spectrum was excited by laser emission wavelength  $\lambda_i = 532.070$  nm. It was shown that  $NV_0$ -center in the input scattering channel makes the largest contribution to the resonance scattering intensity enhancement mechanism [13–15].

We have recently detected the multiband resonant light scattering by optical phonons in homoepitaxial nanoscale  $n$ -GaP layer, 70 nm in thickness, grown on a conducting heavily-doped  $n$ -GaP crystal substrate oriented along [001] axis. Finally, it was shown that, at room temperature in the resonant light scattering spectrum of such (001)  $n$ -GaP nanolayer in  $n$ -GaP/ $n$ -GaP (001) sample compared with the spectrum of high-resistance (001)  $si$ -GaP crystalline sample, two rather narrow lines were detected which were assigned to  $TO(\Gamma)$  phonon vibrations and high-frequency coupled  $LO(\Gamma)+$  plasmon-phonon vibrations. It was found that the spectral parameters of  $LO(\Gamma)+$  vibrations in  $n$ -GaP nanolayer and in (001)  $n$ -GaP substrate differ considerably from each other and from the spectral parameters of  $LO(\Gamma)$  phonon line. The review of the detected strict quantitative features of the spectral parameters allowed for the first time to obtain valuable information about high perfection of a crystal structure with lower density of dislocations and other structural faults. This information is essential for nanoscale epitaxial (001)  $n$ -GaP layer. Methods of measurement of the main electrical properties in semiconductors — concentration  $n$  and mobility  $\mu$  of free charge carriers over  $LO(\Gamma)+$  vibration spectra developed by us earlier [16,17] allowed local values to be measured by a non-contact and non-destructive method. The measured values were equal to

$$n_{\text{hepi}} = (3.25 \pm 0.1) \cdot 10^{17} \text{ cm}^{-3}$$

and mobility

$$\mu_{\text{hepi}} = (40.0 \pm 0.1) \text{ cm}^2 \cdot \text{V}^{-1} \cdot \text{s}^{-1}$$

for homoepitaxial (001)  $n$ -GaP layer compared with  $n_{\text{subs}} = (2.52 \pm 0.1) \cdot 10^{17} \text{ cm}^{-3}$  and  $\mu_{\text{subs}} = (51.0 \pm 0.1) \text{ cm}^2 \cdot \text{V}^{-1} \cdot \text{s}^{-1}$  for (001)  $n$ -GaP substrate of  $n$ -GaP/ $n$ -GaP (001) sample [18,19]. However, it should be noted that creation of device structures on the basis of advanced nanoscale thick homoepitaxial layers grown on heavily-doped substrates is hindered by fairly obvious insurmountable issues of measurement of the degree of crystalline atom structure perfection by traditional X-ray diffraction analysis methods and of electrical properties

investigation by time-consuming methods. The latter require ohmic contacts to be prepared and conductivity and hall effect to be measured. In the frequency range from 600 to 800  $\text{cm}^{-1}$ , rather narrow bands of rather intense second-order light scattering lines associated with various lattice vibration combinations has been detected [19]. It has been found that such bands were caused by total combinations and overtones of transverse and longitudinal optical phonons with wave vectors corresponding to  $\Sigma$ ,  $K$ ,  $X$ ,  $L$  and  $\Gamma$  points of Brillouin zone in GaP crystal. It has been generally shown that for all newly detected lines, light scattering for homoepitaxial  $n$ -GaP layer is of resonant type and is caused by the occurrence of strong exciton-phonon interaction effects. It has been found that such interactions were due to the presence of nitrogen impurities detected by us using the photoluminescence spectra. Interestingly, their presence significantly modifies a well known real energy spectrum of indirect excitons. These representations suggest that such process is directly followed by formation of quasistraight excitons by localized states of the closest nitrogen atom pairs [18,19]. This study describes the results obtained by means of further improvement of the spectrometry procedure for detection of weak light fluxes of separated photons in visible and 0.4–1.35  $\mu\text{m}$  IR ranges. The investigations show, using InAs in (311)B  $si$ -GaAs/InAs structure as an example, that formation of many electronic levels of quantum excitons in heteronanostructures with quantum dots may cause the most strongly pronounced manifestation of activity of new fundamentally essential mechanisms of multiband resonant light scattering. One of the most attractive features of such semiconductor materials with  $\Gamma_8$  degenerate symmetry valence band is strong spin-orbit coupling. Thanks to this coupling, intrinsic moment of holes can interact effectively with the electric field of the incident light wave and cause its adequate scattering. Using the assembly of quantum dots formed in heteroepitaxial (311)B  $si$ -GaAs/InAs system as an example, it was shown that such interaction can cause high light wave scattering by charge carriers and lead to new resonance enhancement mechanisms of inelastic light scattering intensity with specific absolute scattering cross-section and unusual spectral line shape.

## 2. Experimental procedure

An assembly of quantum dots formed in heteroepitaxial (311)B  $si$ -GaAs/InAs system was studied experimentally. It was created on the basis of spontaneous disintegration of heavily strained ultrathin InAs layer grown on (311) GaAs surface into coherent islands. For the purpose of the investigations, specially undoped nanostructures of the self-organized quantum dot assembly were used. Such InAs nanolayers were grown on GaAs surface by a well reproducible method of molecular beam epitaxy on semi-insulating  $si$ -GaAs substrates. Substrates showing  $n$ -type conductivity and oriented along (311)B plane were selected.

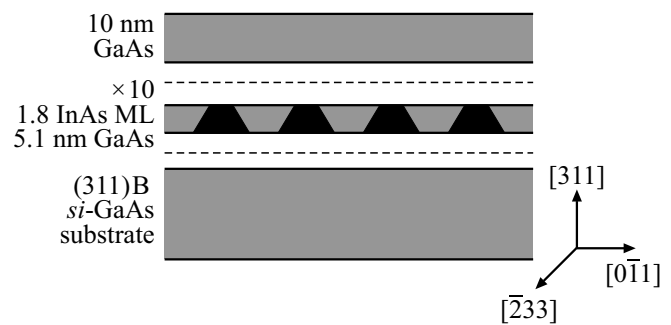


**Figure 1.** Schematic diagram of an assembly of quantum dots formed in heteroepitaxial (311)B  $si$ -GaAs/InAs.

InAs quantum dot islands were directly formed in accordance with Stranski–Krastanov mechanism. For this, the active region of such quantum-dimensional nanostructure was formed by 10 rows of InAs quantum dots. They were directly produced by means of gradual deposition of InAs layers whose thickness was equal to 1.8 monolayer. Such InAs monolayers were separated by GaAs layers whose thickness was equal to 5.1 nm. As a result, the quantum dots in the form of a truncated cone had sizes about 12 and 6 nm. The diagram of the quantum dot structure of interest which was formed in heteroepitaxial (311)B  $si$ -GaAs/InAs system is shown in Figure 1.

Microscopic mechanisms of transition from 2D uniform to spatially-ordered 3D nonuniform growth mode of InAs layers were directly monitored online by variation of typical diffraction pattern of fast electrons reflected from the growing layer surface. Optical investigations of such nanostructures were carried out using the high sensitive spectroscopy procedure for detection of single photons in 0.9–1.35  $\mu\text{m}$  IR range. Inelastic light scattering near IR spectra were excited using highly stable solid-state single-mode continuous wave lasers with active medium on neodymium-doped yttrium-aluminum garnet crystal, with  $\lambda_i = 1064$  nm (line half-width) 0.0004 nm ( ${}^4F_{3/2} - {}^4I_{11/2}$  transition) and with  $\lambda_i = 1318.70$  nm ( ${}^4F_{3/2} - {}^4I_{13/2}$  transition). The study used right-angle grazing beam scattering geometry on (311)B parallel plane sample, with parallel  $[z(yy) - z]$  — hereinafter abbreviated as (HH) and crossed  $[z(yx) - z]$  (HV) polarizations of incident (the first index in parentheses) and scattered (the second index in parentheses) light; the first index before/behind the parenthesis indicates the incident (scattered) light direction, respectively, and  $y$  axis corresponds to  $[233]$  direction and  $x$  axis corresponds to  $[0\bar{1}1]$  direction. For spectral analysis of scattered light, an improved high-power double diffraction spectrometer was used. Instrumental resolution  $R = 3 \text{ cm}^{-1}$ . The test sample was placed on a copper coolant line of the metallic cryostat. For this, a specially built-in calibrated germanium diode operated in a temperature sensor mode was used. Spectra measurements were carried out at helium temperatures. The sample temperature was controlled within  $\pm 0.1$  K. Focused exciting IR emission densities on the sample

within  $P = (0.2-5.0) \text{ kW} \cdot \text{cm}^{-2}$ , were used which did not resulted in any perceptible local heating of the sample. Continuous sample temperature monitoring was provided by means of simultaneous recording and measurement of lattice vibration line frequency corresponding to light scattering by  $\text{LO}(\Gamma)$  and  $\text{LO}(\Gamma)$  phonons from *si*-GaAs substrate and neon spectral lamp emission line. Besides, the detected Stokes and anti-Stokes components of the quasielastic electron light scattering spectrum centered at zero frequency were recorded with analysis of ratio of their absolute intensities. Precision spectroscopy procedure for photon recording also enables important direct control and recording of various possible external factors influencing the light scattering process, including undesired factors. For example, negligible fluctuations of exciting laser power, temperature, pressure etc.

### 3. Experimental findings and discussion

Experimental precision detection of single photons in  $0.9-1.35 \mu\text{m}$  IR range allows to performs high-accuracy measurements of vibrational and electronic states of nanostructures with quantum objects using quantum dots in (311)B *si*-GaAs/InAs heteronanostructures as example. As noted above, the main feature of such cubic semiconductors with  $\Gamma_8$  degenerate valence band is a strong spin-orbit coupling. Thus, the intrinsic moment of holes may effectively interact with the electric field of the incident wave. Such interaction may cause effective light wave scattering of the exciting laser emission and help detect new light scattering mechanisms.

In the photoluminescence spectrum of the nanostructure with InAs quantum dots formed in (311)B *si*-GaAs/InAs system, which was measured using continuous He-Ne laser emission with exciting laser wavelength  $\lambda_i = 632.817 \text{ nm}$ , we have detected a ground electronic exciton transition line at  $E_{ex} = 1.1690 \pm 0.0032 \text{ eV}$  (at  $T = 77 \text{ K}$ ) with half-width (full width at half maximum) of the line equal to  $41.58 \pm 0.08 \text{ eV}$  [20].

In this study, in the photoluminescence spectrum recorded at  $T = 5.2 \text{ K}$  shown in Figure 2, the line maximum with high intensity corresponds to ground exciton state energy  $E_{ex} = 1.1990 \pm 0.0021 \text{ eV}$  (1033.86 nm) with a record-breaking line half-width equal to  $40.15 \pm 0.06 \text{ meV}$ . Exciting laser emission wavelength positions at selective resonant excitation with  $\lambda_i = 1064.15$  and non-resonant excitation with  $\lambda_i = 1318.70 \text{ nm}$  are shown by red and black arrows, respectively.

Thus, it is possible to use continuous neodymium laser emission with  $\lambda_i = 1064.15 \text{ nm}$  for resonant photoexcitation of excitons in InAs quantum dots and  $\lambda_i = 1318.70 \text{ nm}$  laser emission for non-resonant photoexcitation.

Schematic diagram of discrete energy levels of size quantization and emission transitions of light emitted carriers from InAs QD to the ground exciton state ( $1s_e$ -electron state and  $1s_h$ -hole state) in GaAs matrix formed in (311)B

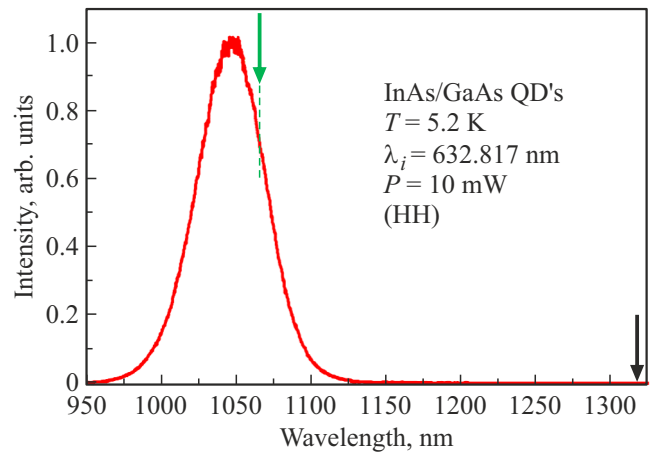


**Figure 2.** photoluminescence spectrum of InAs quantum dots formed in (311)B *si*-GaAs/InAs nanostructure.

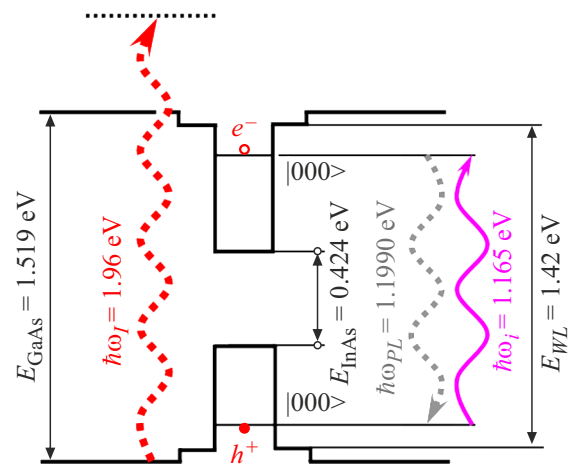


**Figure 3.** Diagram of discrete energy levels of size quantization and transitions between them for InAs quantum dots formed in (311)B *si*-GaAs/InAs system at a sample temperature of  $T_L = 5.2 \text{ K}$ . Selective resonant excitation with  $\hbar\omega_i = 1.1650 \text{ eV}$  ( $\lambda_i = 1064.15 \text{ nm}$ ) frequency is shown by a solid wavy arrow.

*si*-GaAs/InAs hetero-epitaxial system at a sample temperature of  $T_L = 5.2 \text{ K}$  is shown in Figure 3. Here, dashed wavy arrows show exciting emission frequencies of He-Ne laser with  $\hbar\omega_i = 1.96 \text{ eV}$  ( $\lambda_i = 632.817 \text{ nm}$ ) and photoluminescence line maximum with  $\hbar\omega_{PL} = 1.1990 \text{ eV}$  (1033.86 nm) corresponding to exciton.

The first experiments carried out with resonance excitation of this sample at excitation laser wavelength  $\lambda_i = 1064 \text{ nm}$  (quantum energy  $\hbar\omega_i = 1.165 \text{ eV}$ ) with direct excitation from the layer for the studied structure at  $T_L = 5.1 \text{ K}$  compared with the spectra of first-order light scattering by  $\text{TO}(\Gamma)$  phonons at  $271.4 \text{ cm}^{-1}$  and  $\text{LO}(\Gamma)$  phonons at  $294.4 \text{ cm}^{-1}$  obtained for *si*-GaAs substrate (in the same experiment conditions) have shown, as can be clearly seen on the spectrum in Figure 4, that, besides the intense low-frequency region in the frequency range

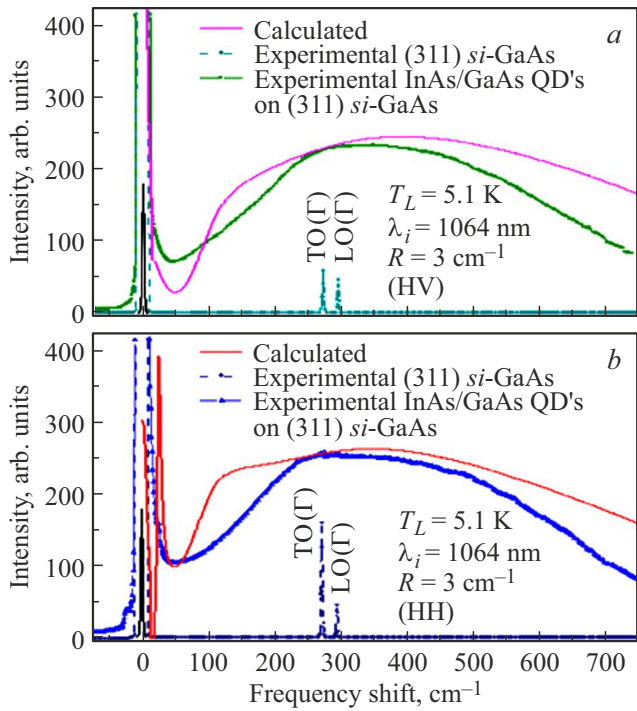


**Figure 4.** Inelastic light scattering spectra found in the heterostructures with InAs quantum dots in (311)B *si*-GaAs/InAs structure in the frequency shift range from  $-75$  to  $750\text{ cm}^{-1}$  with their selective resonant excitation with  $\lambda_i = 1064\text{ nm}$ . Right-angle grazing beam scattering geometry on (311)B parallel plane sample at (a) crossed (HV) and at (b) parallel (HH) polarizations. Solid (red) line — calculations for light scattering on light excited holes in semiconductors with  $\Gamma_8$  degenerate valence band (see the following test). Dashed line — spectrum of first-order light scattering by  $\text{LO}(\Gamma)$  and  $\text{LO}(\Gamma)$  phonons measured in the same experimental conditions for *si*-GaAs substrate.

up to approx.  $50\text{ cm}^{-1}$ , a rather wide dominating band is observed. Such band extends in a sophisticated manner up to the frequency shift range more than  $750\text{ cm}^{-1}$ . A low-frequency region of the observed spectrum approx. from  $-20$  to  $20\text{ cm}^{-1}$  is usually in an experimentally hard-to-reach frequency range directly adjacent to the intense exciting laser line. It definitely demonstrates that a rather intense wing of zero-frequency centered spectrum of quasielastic light scattering by some charge carriers was detected. Such scattering spectrum has a Lorentz profile.

For clarity, low-frequency quasielastic light scattering spectra in near IR frequency range from  $-25$  to  $25\text{ cm}^{-1}$  at a sample temperature of  $T_L = 5.1\text{ K}$  detected by selective resonance excitation with laser wavelength  $\lambda_i = 1064.15\text{ nm}$  and by non-resonance excitation with laser wavelength  $\lambda_i = 1318.70\text{ nm}$  are shown in Figure 5. The same right-angle grazing beam scattering geometry on (311)B parallel plane sample at crossed (HV) and parallel (HH) polarizations of incident and scattered light is shown herein, where the experimental dots are shown by trian-

gles — light (green) for  $\lambda_i = 1064.15\text{ nm}$  and dark (black) for  $\lambda_i = 1318.70\text{ nm}$ .

Figure 6 shows experimental low-temperature spectra of quasielastic light scattering by charge carriers and inelastic light scattering in structures with InAs quantum dots formed in heteroepitaxial (311)B *si*-GaAs/InAs system detected by selective resonance excitation with laser wavelength  $\lambda_i = 1064.15\text{ nm}$  in the frequency range from  $-50$  to  $150\text{ cm}^{-1}$  at a sample temperature  $T_L = 5.1\text{ K}$  (solid line) and (311)B *si*-GaAs substrate (dashed line). Right-angle grazing beam scattering geometry on (311)B parallel plane sample at parallel (HH) polarizations of incident and scattered light was used. These spectra shown in Figure 6 were obtained in the same experimental conditions (temperature, excitation level, polarization, spectral resolution, etc.). Such direct comparison of spectra shown in Figure 6 directly demonstrates that their considerable differences have been found. Interestingly, in the low-temperature

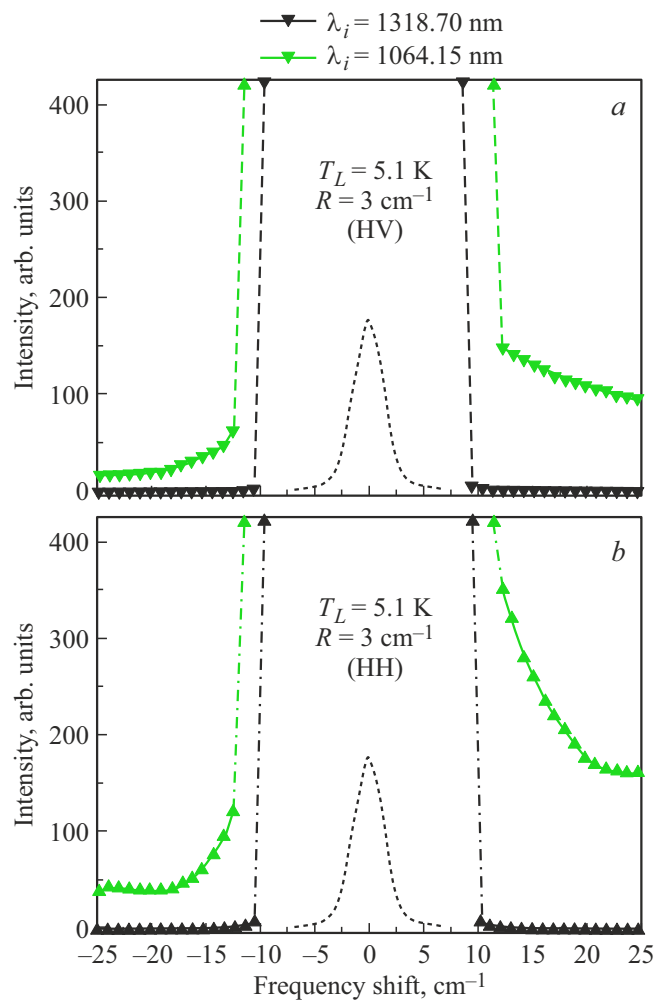


**Figure 5.** Low-temperature spectra of quasielastic light scattering by charge carriers in InAs quantum dot structures formed in (311)B *si*-GaAs/InAs system detected by selective resonance excitation with laser wavelength  $\lambda_i = 1064.15\text{ nm}$  and by non-resonance excitation with laser wavelength  $\lambda_i = 1318.70\text{ nm}$ .

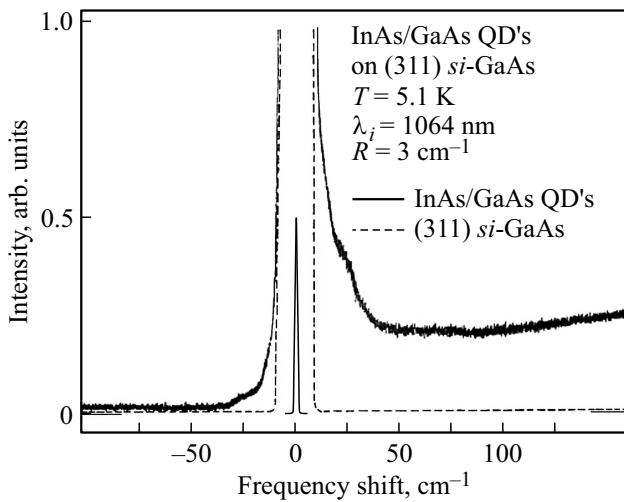


**Figure 6.** Comparison of experimental low-temperature spectra of quasielastic light scattering by charge carriers in structures with InAs quantum dots formed in (311)B *si*-GaAs/InAs system and (311)B *si*-GaAs substrate (dashed line).

spectrum of the test sample, well-defined structures are unexpectedly detected at  $25 \text{ cm}^{-1}$  both in Stokes and anti-Stokes regions. And this feature occurs in (HH) spectra only. We have also found that absolute intensities and profiles of these spectra are very sensitive to the free carrier density and temperature. According to the analysis of our recent interpretations which were initially developed for bulk *n*-InP [14,15] and *p*-GaAs [6–8], and consistent with the sampling procedure (will be addressed later), experimental observation of such spectral feature may be attributed to the acoustic plasmon vibrations of light excited plasma. Direct observation of such acoustic plasmons in two-component electron-hole plasma directly demonstrates that collective excitations are generated in them. It has been also found that the acoustic plasmon structures are only observed in low-temperature spectra. It is possibly due to the fact that light excited electrons and holes may be photoionized and create an exciton cloud of two-component conducting electron-hole plasma (*e*–*h*) in GaAs matrix. It is evident that collective excitations and two-component plasma may exist only in GaAs matrix with embedded InAs quantum dots. Thus, the acoustic plasmon spectra found in the resonance excitation conditions allowed to detect an effective generation of non-equilibrium electron-hole plasma with concentrations  $n = p = 1.0 \cdot 10^{17} \text{ cm}^{-3}$  and temperature  $T_e = T_h = 25 \text{ K}$ , while the lattice temperature is  $T_L = 5.1 \text{ K}$ .

It has been noted above that other new light scattering mechanism may be also detected by selective resonance excitation thanks to strong spin-orbit coupling in structures with InAs quantum dots formed in heteroepitaxial (311)B *si*-GaAs/InAs system with degenerate valence bands. The intrinsic moment of holes can effectively interact with

the electric field of the incident wave leading to inelastic interband and band-to-band light scattering by heavy holes.

It will be shown below that he detected new mechanism can contribute to the formation of the integration complex-profile spectrum of multiplex inelastic light scattering. The spectra in Figure 4 clearly show that such complex-profile spectra may be formed due to overlapping of intense separable resonance contributions. These contributions caused by the quasielastic scattering and scattering by acoustic plasmons of electron-hole plasma as addressed above and by new type inelastic light scattering processes are localized in a wide frequency shift range extending from  $-25$  to more than  $750 \text{ cm}^{-1}$ . Spin-orbit interaction effects addressed herein are small for electrons in GaAs, InAs type semiconductors where spin-orbit coupling is weak in the conduction band. However, they may be significant for holes in semiconductor materials with  $\Gamma_8$  degenerate valence band [21–23]. For holes,  $m_T^* > m_L^*$  condition is met. The number of light holes with weight  $m_L^*$  and, therefore, their contribution to the inelastic light scattering process is negligibly low and, therefore, the major contribution is made by heavy holes. For hole concentration  $N \ll (m_T^* \Delta)^{3/2} / \hbar^3$   $\omega_i \ll E_g / \hbar$ ,  $\Delta$  is the energy of spin-orbit splitting of valence band,  $m_T^*$  is the effective weight of heavy holes,  $E_g = E_{g\Gamma}$  is the straight band gap of semiconductor in point  $\Gamma$  of Brillouin zone (for InAs  $E_{g\Gamma} = 0.417 \text{ eV}$ ), Hamiltonian defining inelastic light scattering in the frequency range  $\omega = \omega_i - \omega_s \ll \Delta / \hbar$  may be written as

$$H_{\text{int}} = e^2 / 2mc^2 \mathbf{A}_i \mathbf{A}_k \mu_{ik}(\mathbf{J}). \quad (1)$$

Here,  $m$  is the free electron mass,  $\mathbf{A}$  is the emission vector potential,  $\mu_{ik}(\mathbf{J})$  is defined by operator matrices  $\mathbf{J}_i$  of the intrinsic hole moment projection as

$$\mu_{ik}(\mathbf{J}) = \gamma_1 \delta_{ik} \mathbf{1} - 2/3 \gamma_2 (3J_i^2 - \mathbf{J}^2) \delta_{ik} - \gamma_3 (1 - \delta_{ik}) (\mathbf{J}_i \mathbf{J}_k + \mathbf{J}_k \mathbf{J}_i). \quad (2)$$

Here,  $\mathbf{1}$  is a single operator,  $\gamma_1$ ,  $\gamma_2$ , and  $\gamma_3$  are Luttinger Hamiltonian defined by operator matrices  $\mathbf{J}_i$  of the intrinsic hole moment projection  $\mu_{ik}(\mathbf{J})$ , where  $\mathbf{p}$  is the quasi-momentum. The detected inelastic light scattering spectra localized in the wide frequency shift range and extending up to more than  $750 \text{ cm}^{-1}$  may be caused by interband and intrasubband transitions of heavy holes which may be observed in the near IR region. Detection of such patterns required experimental implementation of the sharp resonance excitation of near IR spectra. It should be noted that approaches to the construction of the theory of intrasubband light scattering by valence band in semiconductors were first addressed by Ivchenko and Aronov in [24].

For further discussion and generalization of the detected new experimental data with unusually large cross-section and inelastic light scattering spectrum profile and to support the detected new scattering mechanisms, an attempt may be made to take into account the major contributions to the inelastic scattering cross-section of the complex-profile integration multiplex inelastic light scattering spectrum formed by various separable resonance contributions. Such

contributions may occur due to the features of the zone structure of the studied InAs quantum dots in (311)B *si*-GaAs/InAs system. We have found that for this it is necessary to represent the complete expression for light scattering cross-section as the algebraic sum of three light scattering cross-sections for the following addressed mechanisms:

1. quasielastic light scattering by light excited charge carriers,
2. light scattering by acoustic plasmons of electron-hole plasma,
3. inelastic interband and intrasubband light scattering by heavy holes.

Then the complete expression for the light scattering cross-section for cubic point group of symmetry taking into account each of the listed light scattering mechanisms may be, accordingly, written as follows [21–29]:

$$\begin{aligned} \frac{d^2\Sigma}{d\omega d\Omega} = & r_0^2 \frac{3n}{2\varepsilon_{Fh}} \frac{\hbar\omega}{(1 - \exp(\frac{\hbar\omega}{T}))} \left\{ \frac{9\gamma_3^2}{8} \left[ 1 - \left( \frac{\omega}{qV_F} \right)^2 \right]^2 \right. \\ & + \frac{(\mathbf{e}_I \mathbf{e}_S)^2}{L(\omega/qV_F)} + \frac{1}{8} \sqrt{\frac{\hbar\omega}{\gamma_2 \varepsilon_{Fh}}} \\ & \times \int_0^{2\pi} \int_0^\pi \left\{ \frac{f\left(\hbar\omega \frac{\gamma_1 - 2\gamma_2 g(\theta, \phi)}{4\gamma_2 g(\theta, \phi)}\right) - f\left(\hbar\omega \frac{\gamma_1 + 2\gamma_2 g(\theta, \phi)}{4\gamma_2 g(\theta, \phi)}\right)}{\sqrt{g(\theta, \phi)}} \right\} \\ & \times \left[ \gamma_3^2 P(\theta, \phi) I_{\Gamma_{25}}(\mathbf{e}_I, \mathbf{e}_S) + \gamma_2^2 Q(\mathbf{e}_I, \mathbf{e}_S) \right] \sin\theta d\theta d\phi \\ & - \left. \frac{(qr_{FTI})^2 m_e}{\pi m_h} (\mathbf{e}_I \mathbf{e}_S)^2 \text{Im} \varepsilon^{-1}(q, \omega) \right\}. \quad (3) \end{aligned}$$

Here,  $r_0 = e^2/mc^2$  is the traditional electron radius,  $\Omega$  is the solid angle,  $\gamma_1 = 20$ ,  $\gamma_2 = 8.5$  and  $\gamma_3 = 9.2$  [28],  $\varepsilon_{Fh}$  is the Fermi energy for hole,  $\mathbf{e}_I$ ,  $\mathbf{e}_S$  are the polarization vectors for incident and scattered light,  $\omega = \omega_I - \omega_S \ll \Delta/\hbar$  is Stokes frequency shift, and  $\Delta$  is the spin-orbit splitting energy of valence band  $\Delta = 0.39$  eV [30],  $\mathbf{q} = \mathbf{k}_I - \mathbf{k}_S$  is the wave vector transmitted by the light to the electronic system during scattering,  $f(\varepsilon)$  is the Fermi distribution function,  $m_h$  is the effective heavy hole mass,  $L(x) = (\pi x)^2 + 4(1 - x \text{Arth}x)^2$ , ( $\text{Arth}$  — hyperbolic tangent function) depending on the function angle  $g(\theta, \phi)$ ,  $P(\theta, \phi)$  and  $Q(\theta, \phi)$  and depending on function polarization  $I_{\Gamma_{25}}(\mathbf{e}_I, \mathbf{e}_S)$  and  $I_{\Gamma_{12}}(\mathbf{e}_I, \mathbf{e}_S)$  are available in [22,23]. These functions describe two independent so called  $I_{\Gamma_{25}}$  and  $I_{\Gamma_{12}}$  spectra for  $\mathbf{e}_I = (1\bar{1}0)/\sqrt{2}$ ,  $\mathbf{e}_S = (110)/\sqrt{2}$ , and for (100),  $\mathbf{e}_S = (010)$ , respectively.

In the resulting expression (3), taking into account Coulomb interaction between electrons and holes when discrete exciton states will be the intermediate states, each of the summands for these light scattering mechanisms shall

contain a resonance factor [5,7,9,21,22]:

$$R_{ex} = \hbar\omega_i / [E_{ex}^2 - (\hbar\omega_i)^2] [(E_{ex}^2 + \Delta)^2 - (\hbar\omega_i)^2], \quad (4)$$

where  $\Delta$  is the spin-orbit splitting energy of valence band. Such factor in sharp resonance conditions  $\hbar\omega_i \sim E_{ex}$  may result in high observed intensity enhancement for each addressed scattering mechanism taking into account interband and intrasubband transitions between conduction band  $\Gamma_6$ , fourfold degenerate valence band of symmetry  $\Gamma_8$  and doubly degenerate zone  $\Gamma_7$  split by the spin-orbit interaction. Integral intensity of such detected scattering process turned to be abnormally enhanced — more than  $10^5$  times as high as Thomson scattering intensity on charge carriers which is also clearly detected in the observed spectra.

Comparison of the obtained experimental data for the integration multiplex inelastic light scattering spectrum line profile formed due to overlapping of intense separable resonance contributions with evaluation design spectra shown in Figure 4. Dashed lines show good consistency, primarily for difficultly interpretable significant width of the observed inelastic light scattering line.

## 4. Conclusion

This study shows that, using the developed high-sensitive laser spectroscopy methods for inelastic light scattering measurement for detecting separate photons in visible and IR spectra (0.9–1.35  $\mu\text{m}$ ), precision optical investigations of vibrational and electronic states of nanostructures with quantum objects may be carried out using quantum dots in (311)B *si*-GaAs/InAs heterostructures. It is shown that such structures with degenerate valence band of symmetry  $\Gamma_8$  feature strong spin-orbit interaction when the intrinsic moment of holes can effectively interact with the electric field of the incident wave. It has been experimentally demonstrated that such interaction induces light wave scattering and leads to new light scattering mechanisms which have not been observed before. In the IR resonance excitation conditions, intense generation of non-equilibrium electron-hole plasma with concentrations  $n = p = 1.0 \cdot 10^{17} \text{ cm}^{-3}$  and temperature  $T_e = T_h = 25$  K was detected, while the lattice temperature is  $T_L = 5.1$  K. New formation mechanisms of an abnormally intense integration complex-profile spectrum of multiplex inelastic light scattering were detected. It is shown that such spectrum profile may be formed due to manifestation of various resonance contributions of quasielastic electronic scattering and scattering by acoustic plasmons of electron-hole plasma, and of inelastic interband and intrasubband light scattering by heavy holes in near IR region. The abnormal resonance intensity enhancement of such scattering is found to be more than  $10^5$  times as high as Thomson scattering on charge carriers for a bulk material. Consistency is observed between the design and experimental spectra, primarily for difficultly interpretable profile and significant width of the detected inelastic light scattering spectral line.

In general, the obtained unique photophysical properties of solid-state multicomponent plasma of InAs quantum dots in GaAs matrix show that the determined new resonance mechanisms of various contributions to scattered photon emission are essential diagnostic components clearly manifested in the resulting inelastic electronic light scattering spectra. Such results open new opportunities for implementation of possible optical spin state control circuits in a wide range of new experiments and process applications. They are of interest for the development of important promising semiconductor spintronics, quantum optics and metrology areas, because they significantly increase analytical capabilities of the optical spectroscopy. They are also important for the creation of quantum information technology hardware components and are also of interest for solution of high-priority fundamental and application modern physics problems such as the development of extra contrast single-photon IR emission sources and new spectroscopy plasma diagnostics approaches.

### Acknowledgments

The authors express their sincere gratitude to V.A. Voitenko for multiple useful discussions of the findings and spectral line profile assessments.

### Conflict of interest

The authors declare that they have no conflict of interest.

### References

- [1] R. Loudon. Proc. R. Soc. A **275**, 218 (1963).
- [2] A.K. Ganguly, J.L. Birman. Phys. Rev. **162**, 806 (1967).
- [3] R.M. Martin. Phys. Rev. B **4**, 3676 (1971).
- [4] R. Zeyher, T. Chiu-Sen, J.L. Birman. Phys. Rev. B **4**, 1725 (1974).
- [5] Light Scattering in Solids. Topics in Applied Physics / Ed. M. Cardona, G. Guntherodt. Springer, Berlin, Heidelberg, N.Y. (1974). 543 p.
- [6] B.H. Bairamov, A.V. Gol'tsev, E. Karaiamaki, R. Laikho, T. Levola, V.V. Toporov. Sov. Phys. Solid State **25**, 739 (1983).
- [7] E. Karajamaki, R. Laiho, T. Levola, B.H. Bairamov, A.B. Gol'tsev, V.V. Toporov. Phys. Rev. B **29**, 4508 (1984).
- [8] B.H. Bairamov, N.V. Lichkova, A.B. Gol'tsev, V.D. Timofeev, V.V. Toporov. Sov. Phys. Solid State **29**, 244 (1987). [Fiz. Tverd. Tela, **29**, 754 (1987)].
- [9] A. Cantarero, C. Trallero-Giner, M. Cardona. Phys. Rev. B **39**, 8388 (1989).
- [10] C. Trallero-Giner, K. Syassen. Phys. Status Solidi B **247**, 182 (2010).
- [11] R.P. Miranda, M.I. Vasilevskiy, C. Trallero-Giner. Phys. Rev. B **74**, 115317 (2006).
- [12] F.B. Bairamov, V.V. Toporov, E.D. Poloskin, B.Kh. Bairamov, C. Röder, C. Sprung, C. Bohmhammel, G. Seidel, G. Irmer, A. Lashkul, E. Lahderanta, Y.W. Song. FTP **47**, 607 (2013).
- [13] B.H. Bairamov, V.V. Toporov, F.B. Bayramov, A.D. Bouravleuv, J.T. Holmi, H. Lipsanen, V.P. Popov, I.N. Kuprianov, Yu.N. Pal'anov, D. Braukmann, J. Debus, D.R. Yakovlev, M. Bayer. Sibir. Phys. J. **13**, 3, 73 (2018).
- [14] B.Kh. Bairamov, V.V. Toporov F.B. Bairamov. FTP, **53**, 85 (2019). (in Russian).
- [15] B.H. Bairamov, V.V. Toporov, F.B. Bayramov. Semicond. **53**, 16, 2129 (2019).
- [16] B.H. Bairamov, A. Heinrich, G. Irmer, V.V. Toporov, E. Ziegler. Phys. Status Solidi B **119**, 227 (1983).
- [17] G. Irmer, V.V. Toporov, B.H. Bairamov, J. Monecke. Phys. Status Solidi B **119**, 595 (1983).
- [18] B.Kh. Bairamov, V.V. Toporov F.B. Bairamov. FTT **63**, 1, 80 (2021). (in Russian).
- [19] B.Kh. Bairamov. FTT **63**, 2, 213 (2021). (in Russian).
- [20] Y.A. Kuznetsova, F.B. Bayramov, V.V. Toporov, B.H. Bairamov, A.P. Glinushkin, V.Yu. Rud. IOP Conf. Ser.: Earth Environ. Sci. 1096 012032 (2022).
- [21] V.A. Voitenko. FTT **26** 1002 (1984). (in Russian).
- [22] V.A. Voitenko. FTT **28** 3091 (1986). (in Russian).
- [23] B.H. Bairamov, I.P. Ipatova, V.A. Voitenko. Phys.Rep. **229**, 5, 221 (1993).
- [24] A.G. Aronov, E.L. Ivchenko ZhETF **57**, 247 (1969). (in Russian).
- [25] B.Kh. Bairamov, V.A.Voitenko, I.P. Ipatova. UFN **163**, 5, 67 (1993). (in Russian).
- [26] V.A. Voitenko. Pis'ma v ZhETF **61**, 91 (1995). (in Russian).
- [27] B.H. Bairamov, I.P. Ipatova, V.A. Voitenko, V.K. Negoduyko, V.V. Toporov. Phys. Rev. B **50**, 20, 14923 (1994).
- [28] B.H. Bairamov, V.A. Voitenko, V.V. Toporov, B.P. Zakharchenya, M. Henini, A.J. Kent. Nanotechnology **11**, 4, 314 (2000).
- [29] V.A. Voitenko. Private Commun.
- [30] I. Vurgaftman, J.R. Meyer, L.R. Ram-Mohan. J. Appl. Phys. **89**, 11, 5815 (2001).

Translated by E.Ilyinskaya